LOCAL REFINEMENT FOR 3D DEFORMABLE PARAMETRIC SURFACES

Anaïs Badoual, Daniel Schmitter, and Michael Unser

Biomedical Imaging Group, École Polytechnique Fédérale de Lausanne (EPFL), Switzerland

ABSTRACT

Biomedical image segmentation is an active field of research where deformable models have proved to be efficient. The geometric representation of such models determines their ability to approximate the shape of interest as well as the speed of convergence of related optimization algorithms. We present a new tensor-product parameterization of surfaces that offers the possibility of local refinement. The goal is to allocate additional degrees of freedom to the surface only where an increase in local detail is required. We introduce the possibility of locally increasing the number of control points by inserting basis functions at specific locations. Our approach is generic and relies on refinable functions which satisfy the refinement relation. We show that the proposed method improves brain segmentation in 3D MRI images.

Index Terms— deformable model, parametric surface, refinable function, local refinement, segmentation, splines.

1. INTRODUCTION

A crucial aspect in the development of local refinement algorithms is to refine specific regions while keeping the rest of the surface unchanged. This local refinement is not inherent to standard methods as Non-Uniform Rational Basis Splines (NURBS) or classical parameterizations of tensor-product surfaces. Existing methods to insert points at specific locations were developped in [1, 2, 3, 4, 5]. We propose a new generic tensor-product parameterization for surfaces where the degrees of freedom can be locally increased without altering the shape of the surface. We locally improve the level of detail of the parametric model by inserting basis functions at specific locations. Our approach relies on refinable functions and the property that cardinal B-splines can be implemented efficiently using digital filters.

The motivation for this work is the improved design of deformable models for biomedical image analysis. Deformable models are flexible curves or surfaces that are deformed in order to approximate a specific shape. They can be modelled explicitly by parameterizations [6] and meshes [7], or implicitly by level sets [8]. Parametric and mesh representations facilitate a direct user interaction with the model. The deformation is controlled manually by interactively varying the parameters of the model or automatically by minimizing an energy functional [6, 9]. Deformable models have been applied successfully for image segmentation, tracking and face recognition [10, 11, 12]. In the medical field, they are used for 3D visualization for surgical planning or to detect morphological changes of a specific anatomic structure over time. In biomedical imaging it is desirable to limit the number of parameters of the model to speed up the computation. When dealing with complex shapes, classical deformable parametric surfaces [13] use a global approach to add more details. This globally increases the number of degrees of freedom of the model. A precise location of the insertion of the additional control points is preferable for a fast optimization, which is precisely what our proposed local refinement scheme deals with.

This paper extends the theory that was developed for 2D locally refinable parametric snakes [14]. The main contribution here is a generic formulation of 3D locally refinable parametric surfaces that can be used with any valid refinable function. It can be applied to deformable models where the energy usually is independent of the parameterization [13]. We illustrate the proposed scheme by presenting its application to the semi-automatic segmentation of the brain in 3D MRI.

2. LOCALLY REFINABLE PARAMETRIC SURFACES

2.1. Notation

We denote by t a continuous parameter in $\mathbb{R}$. We define $\boldsymbol{\alpha} = (\alpha_1, \alpha_2, \ldots, \alpha_L)$ and denote by L_n the multiplicity of the element $\alpha_n \in \boldsymbol{\alpha}$, for $n = 1, \ldots, L$. We denote by $\varphi_{\boldsymbol{\alpha}}$ a function that reproduces exponential polynomials in $\operatorname{span}\{\mathrm{e}^{\alpha_n t}, \ldots, t^{L_n-1}\mathrm{e}^{\alpha_n t}\}_{n=1,\ldots,L}$, as for instance exponential B-splines do [15].

2.2. Generic Representation of Tensor-Product Surfaces

A 3D surface $\boldsymbol{\sigma}$ is described by a triplet of coordinate functions $(x(u,v), y(u,v), z(u,v))$, where $u, v \in \mathbb{R}$ are continuous parameters. Each coordinate function is parameterized by a suitable linear combination of integer-shifted separable basis functions $\{\varphi_{\boldsymbol{\alpha}_1}(u-k)\varphi_{\boldsymbol{\alpha}_2}(v-l)\}_{k,l\in\mathbb{Z}}$ weighted by a

This work was funded by the Swiss National Science Foundation under Grant 200020-162343.

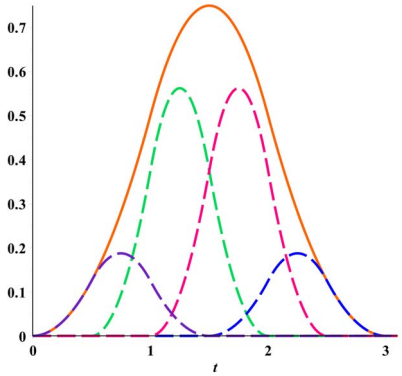

Fig. 1. Refinement of a quadratic B-spline with a refinement factor m equal to 2 (orange line). It can be expressed as a linear combination of four contracted versions (dashed lines) of integer-shifted quadratic B-splines.

sequence of control points $\{c[k,l]\}_{k,l\in\mathbb{Z}}$. The functions $\varphi_{\boldsymbol{\alpha}_1}$ and $\varphi_{\boldsymbol{\alpha}_2}$ determine the shapes that the parametric surface can adopt. Then, the parametric representation of the surface is given by the equation

$$\begin{aligned}\boldsymbol{\sigma}(u,v) &= \begin{pmatrix} x(u,v) \\ y(u,v) \\ z(u,v) \end{pmatrix} \\ &= \sum_{k\in\mathbb{Z}}\sum_{l\in\mathbb{Z}} \mathbf{c}[k,l]\varphi_{\boldsymbol{\alpha}_1}(u-k)\varphi_{\boldsymbol{\alpha}_2}(v-l),\end{aligned} \tag{1}$$

where $\{\mathbf{c}[k,l] = (c_x[k,l], c_y[k,l], c_z[k,l])\}_{k,l\in\mathbb{Z}}$ are the 3D control points describing the shape. In practice, the generators $\varphi_{\boldsymbol{\alpha}_1}$ and $\varphi_{\boldsymbol{\alpha}_2}$ are chosen to be compactly-supported. Then, the surface can be modified locally by displacing a single control point.

2.3. Refinable Functions

We define by $\{h_{\boldsymbol{\alpha},m}[k]\}_{k\in\mathbb{Z}}$ the coefficients of the refinement filter [16, 17]. The generator $\varphi_{\boldsymbol{\alpha}}$ is called a *refinable function* if it verifies the refinement relation given by

$$\varphi_{\boldsymbol{\alpha}}(\frac{t}{m}) = \sum_{k\in\mathbb{Z}} h_{\frac{\boldsymbol{\alpha}}{m},m}[k]\varphi_{\frac{\boldsymbol{\alpha}}{m}}(t-k), \tag{2}$$

where m is called the *refinement factor*. The non-standard aspect here is the fact that the scheme is "non-stationary", meaning that the basis functions on both sides of (2) involve different parameters, *i.e.*, $\boldsymbol{\alpha}$ and $\frac{\boldsymbol{\alpha}}{m}$. If $\varphi_{\boldsymbol{\alpha}}$ is a valid refinable function its dilatation by m can be expressed as a linear combination of the integer shifts of the generator $\varphi_{\frac{\boldsymbol{\alpha}}{m}}$. Examples of such functions are B-splines [15] or the sinc function. In Figure 1 we illustrate the refinenement of a quadratic B-spline for $m = 2$ whose corresponding refinement filter is defined by its z-transform as $H_{(0,0,0),2}(z) = \frac{1}{4}(1+z^{-1})^3$.

2.4. Local Refinement of $\boldsymbol{\sigma}$

In this section, we describe our main contribution which consists of the formulation of a locally refined parametric surface. We use refinable functions as generators $\varphi_{\boldsymbol{\alpha}_1}$ and $\varphi_{\boldsymbol{\alpha}_2}$ to construct surfaces described by (1). We apply the refinement relation (2) locally, *i.e.*, only with respect to the particular control point $\mathbf{c}[p,q]$ associated to the basis functions $\varphi_{\boldsymbol{\alpha}_1}(u-p)$ and $\varphi_{\boldsymbol{\alpha}_2}(v-q)$. The refinement factors are equal to m_1 and m_2 in the directions u and v, respectively.

Proposition 1. *A locally refined parametric tensor-product surface is expressed as*

$$\begin{aligned}\boldsymbol{\sigma}(u,v) = &\sum_{\substack{(k,l)\in\mathbb{Z}^2 \\ (k,l)\neq(p,q)}} \mathbf{c}[k,l]\varphi_{\boldsymbol{\alpha}_1}(u-k)\varphi_{\boldsymbol{\alpha}_2}(v-l) \\ &+ \sum_{i=l_1}^{l_1+N_1-1}\sum_{j=l_2}^{l_2+N_2-1} \tilde{\mathbf{c}}_{p,q}[i,j]\varphi_{\frac{\boldsymbol{\alpha}_1}{m_1}}(m_1u-m_1p-i) \\ &\times \varphi_{\frac{\boldsymbol{\alpha}_2}{m_2}}(m_2v-m_2q-j),\end{aligned} \tag{3}$$

where N_1 and N_2 are the sizes of the discrete filters $h_{\frac{\boldsymbol{\alpha}_1}{m_1},m_1}$ and $h_{\frac{\boldsymbol{\alpha}_2}{m_2},m_2}$, respectively, whose supports are $[l_1, l_1+N_1-1]$ and $[l_2, l_2+N_2-1]$, and $\tilde{\mathbf{c}}_{p,q}[i,j] = \mathbf{c}[p,q]h_{\frac{\boldsymbol{\alpha}_1}{m_1},m_1}[i]h_{\frac{\boldsymbol{\alpha}_2}{m_2},m_2}[j]$. Thereby, p and q are freely chosen.

Proof: Using (1) we write

$$\begin{aligned}\boldsymbol{\sigma}(u,v) = &\sum_{\substack{(k,l)\in\mathbb{Z}^2 \\ (k,l)\neq(p,q)}} \mathbf{c}[k,l]\varphi_{\boldsymbol{\alpha}_1}(u-k)\varphi_{\boldsymbol{\alpha}_2}(v-l) \\ &+ \underbrace{\mathbf{c}[p,q]\varphi_{\boldsymbol{\alpha}_1}(u-p)\varphi_{\boldsymbol{\alpha}_2}(v-q)}_{\boldsymbol{\sigma}_{p,q}(u,v)}.\end{aligned} \tag{4}$$

Using the refinement property (2) we obtain

$$\begin{aligned}\boldsymbol{\sigma}_{p,q}(u,v) &= \mathbf{c}[p,q]\sum_{i\in\mathbb{Z}} h_{\frac{\boldsymbol{\alpha}_1}{m_1},m_1}[i]\varphi_{\frac{\boldsymbol{\alpha}_1}{m_1}}(m_1u-m_1p-i) \\ &\times \sum_{j\in\mathbb{Z}} h_{\frac{\boldsymbol{\alpha}_2}{m_2},m_2}[j]\varphi_{\frac{\boldsymbol{\alpha}_2}{m_2}}(m_2v-m_2q-j) \\ &= \sum_{i\in\mathbb{Z}}\sum_{j\in\mathbb{Z}} \underbrace{\mathbf{c}[p,q]h_{\frac{\boldsymbol{\alpha}_1}{m_1},m_1}[i]h_{\frac{\boldsymbol{\alpha}_2}{m_2},m_2}[j]}_{\tilde{\mathbf{c}}_{p,q}[i,j]}\varphi_{\frac{\boldsymbol{\alpha}_1}{m_1}}(m_1u-m_1p-i) \\ &\times \varphi_{\frac{\boldsymbol{\alpha}_2}{m_2}}(m_2v-m_2q-j).\end{aligned} \tag{5}$$

To simplify the infinite sums in (5) we take into account the size of the filters $h_{\frac{\boldsymbol{\alpha}_1}{m_1},m_1}$ and $h_{\frac{\boldsymbol{\alpha}_2}{m_2},m_2}$, which is equal to N_1 and N_2, respectively, as well as their localization on $[l_1, l_1+N_1-1]$ and $[l_2, l_2+N_2-1]$. We obtain

$$\begin{aligned}\boldsymbol{\sigma}_{p,q}(u,v) = &\sum_{i=l_1}^{l_1+N_1-1}\sum_{j=l_2}^{l_2+N_2-1} \tilde{\mathbf{c}}_{p,q}[i,j] \\ &\times \varphi_{\frac{\boldsymbol{\alpha}_1}{m_1}}(m_1u-m_1p-i)\varphi_{\frac{\boldsymbol{\alpha}_2}{m_2}}(m_2v-m_2q-j).\end{aligned} \tag{6}$$

By combining (4) and (6), we obtain (3). ■

Therefore, as the basis functions $\varphi_{\boldsymbol{\alpha}_1}$ and $\varphi_{\boldsymbol{\alpha}_2}$ are compactly supported, the infinite sums in (3) can be reduced to finite ones where the limits depend on the size of their support. One can refine the surface at several specific locations by applying Proposition 1 with respect to each corresponding control point.

The local refinement described by Proposition 1 leaves the surface unchanged. The part $\boldsymbol{\sigma}_{p,q}$ of the surface initially controlled by $\mathbf{c}[p,q]$ is now described by $(N_1 \times N_2)$ new control points $\{\tilde{\mathbf{c}}_{p,q}[i,j]\}_{i\in[l_1,\ldots,l_1+N_1-1],j\in[l_2,\ldots,l_2+N_2-1]}$; each of them controls a small part of $\boldsymbol{\sigma}_{p,q}$. We thus increase the approximation power of the surface at the specific region $\boldsymbol{\sigma}_{p,q}$ which can be modified more accurately. By approximation power we mean the ability of the model to approximate a shape with accuracy. The error of approximation decreases when the number of parameters increases [18]. In Figure 2, we compare the proposed method to the global approach used with classical parametric snakes to increase the approximation power at a specific region of the surface. In Figure 3, we illustrate a local refinement on a cylindrical surface constructed with exponential B-splines. We show the influence of the refinement for each direction u and v in Figure 4.

In the following section, we illustrate the advantages of the proposed local refinement with a specific application.

3. PRACTICAL APPLICATION: SEMI-AUTOMATIC BRAIN SEGMENTATION

The proposed local refinement can be efficiently exploited for the construction of deformable models, as it was presented in the 2D case in [14]. For instance, our new formulation can be applied to the energies proposed in [13]. Brain segmentation algorithms are used in medicine to visualize the organ for surgical planning or to detect temporal morphological changes in relation with neurological diseases [19]. The brain is a complex structure with many concavities such as lobes or grooves. In this section, we perform a refined brain segmentation in a 3D MRI volume using a deformable model with spherical topology.

3.1. Surface with Spherical Topology

We use the parameterization proposed by [20] which is a tensor-product surface with spherical topology specified by

$$\boldsymbol{\sigma}(u,v) = \begin{pmatrix} \cos(2\pi u)\sin(\pi v) \\ \sin(2\pi u)\sin(\pi v) \\ \cos(\pi v) \end{pmatrix} = \sum_{k=0}^{M_1-1} \sum_{l=-2}^{M_2-1} \mathbf{c}[k,l]\varphi_{\boldsymbol{\alpha}_1,M_1}(M_1u-k)\varphi_{\boldsymbol{\alpha}_2}(M_2v-l),$$

where $u,v \in [0,1]$ and the function $\varphi_{\boldsymbol{\alpha}_1,M_1}$ is the M_1-periodization of the function $\varphi_{\boldsymbol{\alpha}_1}$ defined as $\varphi_{\boldsymbol{\alpha}_1,M_1}(t) =$

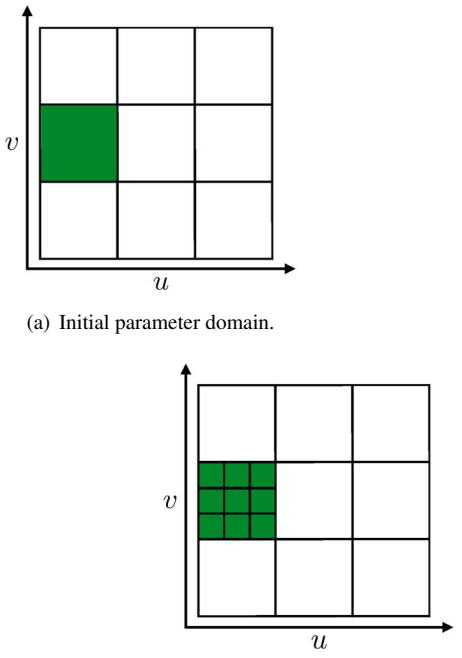

(a) Initial parameter domain.

(b) Global approach.

(c) Local refinement.

Fig. 2. Increase of the approximation power of the region $\boldsymbol{\sigma}_{p,q}$ (green region) by locally adding nodes to the parameter domain. We compare the global approach used with classical parametric snakes and the proposed method. (a): initial configuration; (b): configuration obtained after globally increasing by a factor 3 the number of control points in each direction. The entire parameter domain is affected; (c): configuration obtained by applying a local refinement with respect to the control point $\mathbf{c}[p,q]$ with $m_1 = m_2 = 3$. The region $\boldsymbol{\sigma}_{p,q}$ is divided into 9 areas, whereas the rest of the parameter domain remains unchanged.

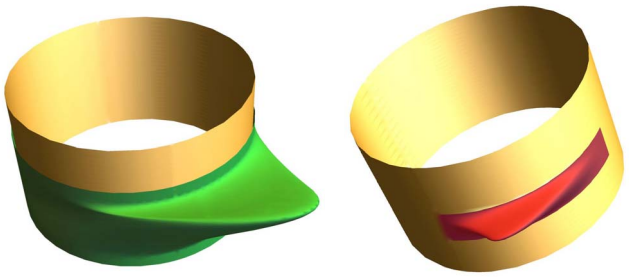

(a) Surface $\boldsymbol{\sigma}_{p,q}$.

(b) Refinement of the surface $\boldsymbol{\sigma}_{p,q}$.

Fig. 3. The deformation of a cylinder (yellow) by displacement of the control point $\mathbf{c}[p,q]$ alters a large region $\boldsymbol{\sigma}_{p,q}$ of the surface ((a), green surface). A local refinement with respect to $\mathbf{c}[p,q]$ allows to accurately control a specific part of $\boldsymbol{\sigma}_{p,q}$ ((b), red surface).

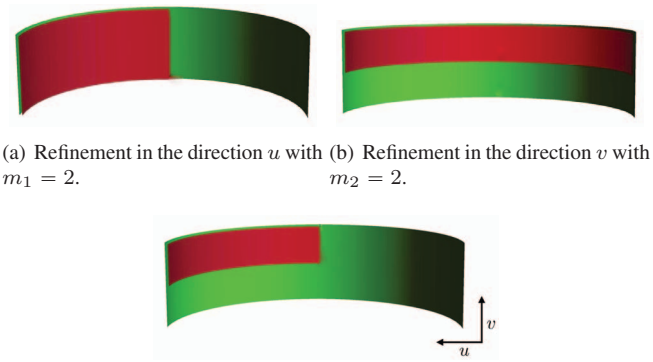

(a) Refinement in the direction u with $m_1 = 2$.

(b) Refinement in the direction v with $m_2 = 2$.

(c) Refinement in both directions u and v with $m_1 = 2$ and $m_2 = 2$.

Fig. 4. Refinement of the region $\boldsymbol{\sigma}_{p,q}$ (green surface) of the cylinder with respect to $\mathbf{c}[p,q]$ performed in direction u in (a), v in (b) as well as in both directions in (c). Red pattern: surface controlled by one of the new points $\tilde{\mathbf{c}}_{p,q}$.

$\sum_{n\in\mathbb{Z}} \varphi_{\boldsymbol{\alpha}_1}(t - nM_1)$. The generators $\varphi_{\boldsymbol{\alpha}_1}$ and $\varphi_{\boldsymbol{\alpha}_2}$ are the causal versions of the functions used in [20] defined as $\varphi_{\boldsymbol{\alpha}_i} = \lambda_i \beta_{\boldsymbol{\alpha}_i}$, for $i = 1, 2$, where the functions $\beta_{\boldsymbol{\alpha}_i}$ are exponential B-splines characterized by their vector of poles $\boldsymbol{\alpha}_1 = \{0, \frac{j2\pi}{M_1}, \frac{-j2\pi}{M_1}\}$ and $\boldsymbol{\alpha}_2 = \{0, \frac{j\pi}{M_2}, \frac{-j\pi}{M_2}\}$, and $\lambda_i = (\mathrm{sinc}\, \frac{1}{M_i})^{-2}$ is a coefficient that ensures the affine invariance of the model. The causal exponential B-spline $\beta_{\boldsymbol{\alpha}}$ is defined in the frequency domain by $\hat{\beta}_{\boldsymbol{\alpha}}(\omega) = \prod_{n=1}^{L} \frac{1-e^{\alpha_n - j\omega}}{j\omega - \alpha_n}$ [15]. For the experiment we use $M_1 = M_2 = 8$, which leads to a total number of 52 control points instead of 76 in [20], and $m_1 = m_2 = 2$. The corresponding refinement filters $h_{\boldsymbol{\alpha}_1,m_1}$ and $h_{\boldsymbol{\alpha}_2,m_2}$ have a support of size 4 and are defined by their z-transform as $H_{\boldsymbol{\alpha}_i,m_i}(z) = \frac{1}{m_i^2} \prod_{n=1}^{3} (\sum_{q=0}^{m_i-1} e^{\alpha_{i_n} q} z^{-q})$. Equation (3) in Proposition 1 is expressed as

$$
\begin{aligned}
\boldsymbol{\sigma}(u,v) = & \sum_{\substack{k=0 \\ k\neq p}}^{M_1-1} \sum_{l=-2}^{M_2-1} \mathbf{c}[k,l] \varphi_{\boldsymbol{\alpha}_1,M_1}(M_1 u - k) \varphi_{\boldsymbol{\alpha}_2}(M_2 v - l) \\
& + \sum_{\substack{l=-2 \\ l\neq q}}^{M_2-1} \mathbf{c}[p,l] \varphi_{\boldsymbol{\alpha}_1,M_1}(M_1 u - p) \varphi_{\boldsymbol{\alpha}_2}(M_2 v - l) \\
& + \sum_{i=0}^{3} \sum_{j=0}^{3} \tilde{\mathbf{c}}_{p,q}[i,j] \varphi_{\frac{\boldsymbol{\alpha}_1}{2},2M_1}(2M_1 u - 2p - i) \\
& \times \varphi_{\frac{\boldsymbol{\alpha}_2}{2}}(2M_2 v - 2q - j),
\end{aligned}
$$

where $\tilde{\boldsymbol{c}}_{p,q}[i,j] = \mathbf{c}[p,q] h_{\frac{\boldsymbol{\alpha}_1}{2},2}[i] h_{\frac{\boldsymbol{\alpha}_2}{2},2}[j]$.

3.2. Experiment

In order to have a fast and accurate delineation of the brain, we perform the segmentation in three steps. First, we optimize a classical active surface with few parameters in order to obtain a fast rough outline of the brain. Then, we manually perform a local refinement. Finally, we optimize a second time by interactively moving the new control points.

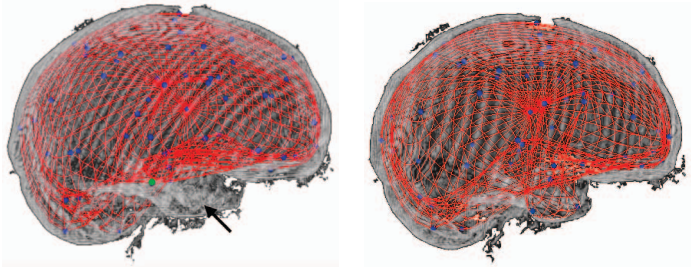

(a) Brain segmentation without local refinement. Green sphere: $\mathbf{c}[1,5]$.

(b) Accurate brain segmentation after local refinement.

Fig. 5. Semi-automatic brain segmentation on a 3D MRI volume using the proposed local refinement. Red: snake; Spheres: control points. Arrow in (a): lobe of the brain not accurately segmented.

For the first step, we use the automatic 3D parametric snake based on a spherical topology described in [20] and with the parameters given in Section 3.1. Thanks to the few control points used, we obtain a faster algorithm (60 seconds) than the one presented in [20] which uses a global approach. We provide the segmentation result in Figure 5 (a). We observe that one of the lobes of the brain is not accurately segmented as it exhibits fine details. Then, we perform a local refinement with respect to the control point $\mathbf{c}[1,5]$ as it controls the part of the surface that we want to deform in order to well segment the lobe. The region initially controlled by $\mathbf{c}[1,5]$ is now divided into 16 smaller areas controlled by the new control points $\{\tilde{\mathbf{c}}_{1,5}[i,j]\}_{i,j\in[0,\ldots,3]}$. We thus locally gain in approximation power and accuracy. Finally, the snake is deformed by displacement of the points $\tilde{\mathbf{c}}_{1,5}$ in order to delineate the lobe. The segmentation result obtained is given in Figure 5 (b). We can see that the lobe is finally accurately segmented.

4. CONCLUSION

We have presented a new parameterization of locally refinable and deformable surfaces. Our motivation is for 3D image segmentation. Our method is generic and can be used with any refinable function. The goal is to increase the number of parameters of the model only where it is necessary. This avoids an optimization with an excess of parameters which speeds up computation, while enhancing flexibility. We illustrated the proposed local refinement and its ability to improve segmentation results with a practical application.

5. REFERENCES

[1] T. W. Sederberg, D. L. Cardon, G.T. Finnigan, N.S. North, J. Zheng, and T. Lyche, "T-spline simplification

and local refinement," *ACM Trans. Graph.*, vol. 23, no. 3, pp. 276–283, Aug. 2004.

[2] C. Giannelli, B. Jüttler, and H. Speleers, "Strongly stable bases for adaptively refined multilevel spline spaces," *Adv. Comput. Math.*, vol. 40, no. 2, pp. 459–490, 2014.

[3] T. Dokken, T. Lyche, and K. F. Pettersen, "Polynomial splines over locally refined box-partitions.," *Computer Aided Geometric Design*, vol. 30, no. 3, pp. 331–356, 2013.

[4] C. Giannelli, B. Jüttler, and H. Speleers, "THB-splines: The truncated basis for hierarchical splines.," *Computer Aided Geometric Design*, vol. 29, no. 7, pp. 485–498, 2012.

[5] C. Manni, F. Pelosi, and H. Speleers, "Local Hierarchical h-Refinements in IgA Based on Generalized B-Splines," *Mathematical Methods for Curves and Surfaces*, vol. 8177, pp. 341–363, 2014.

[6] M. Kass, A. Witkin, and D. Terzopoulos, "Snakes: Active contour models," *International Journal of Computer Vision*, vol. 1, no. 4, pp. 321–331, January 1987.

[7] V. Blanz and T. Vetter, "A morphable model for the synthesis of 3D faces," in *Proceedings of the 26th Annual Conference on Computer Graphics and Interactive Techniques*, New York, NY, USA, 1999, SIGGRAPH '99, pp. 187–194, ACM Press/Addison-Wesley Publishing Co.

[8] V. Caselles, R. Kimmel, and G. Sapiro, "Geodesic active contours," *International Journal of Computer Vision*, vol. 22, no. 1, pp. 61–79, 1997.

[9] X. Bresson, S. Esedoglu, P. Vandergheynst, J.-P. Thiran, and S. Osher, "Fast global minimization of the active contour/snake model," *Journal of Mathematical Imaging and Vision*, vol. 28, no. 2, pp. 151–167, 2007.

[10] B. De Leener, S. Kadoury, and J. Cohen-Adad, "Robust, accurate and fast automatic segmentation of the spinal cord," *NeuroImage*, vol. 98, pp. 528–536, September 2014.

[11] A. Dufour, R. Thibeaux, E. Labruyere, N. Guillen, and J.-C. Olivo-Marin, "3-D Active meshes: Fast discrete deformable models for cell tracking in 3-D time-lapse microscopy," *IEEE Transactions on Image Processing*, vol. 20, no. 7, pp. 1925–1937, July 2011.

[12] G. Székely, A. Kelemen, C. Brechbhler, and G. Gerig, "Segmentation of 2D and 3D objects from MRI volume data using constrained elastic deformations of flexible fourier contour and surface models," *Medical Image Analysis*, vol. 1, no. 1, pp. 19–24, March 1996.

[13] D. Schmitter, C. Gaudet-Blavignac, D. Piccini, and M. Unser, "New parametric 3D snake for medical segmentation of structures with cylindrical topology," in *Proceedings of the 2015 IEEE International Conference on Image Processing (ICIP'15)*, Québec QC, Canada, September 27-30, 2015, pp. TEC–P21.2.

[14] A. Badoual, D. Schmitter, and M. Unser, "Locally refinable parametric snakes," in *Proceedings of the 2015 IEEE International Conference on Image Processing (ICIP'15)*, Québec QC, Canada, September 27-30, 2015, pp. TEC–P21.2.

[15] M. Unser and T. Blu, "Cardinal exponential splines: Part I—Theory and filtering algorithms," *IEEE Transactions on Signal Processing*, vol. 53, no. 4, pp. 1425–1438, April 2005.

[16] Costanza Conti and Lucia Romani, "Algebraic conditions on non-stationary subdivision symbols for exponential polynomial reproduction," *Journal of Computational and Applied Mathematics*, vol. 236, no. 4, pp. 543 – 556, 2011.

[17] L. Romani, "From approximating subdivision schemes for exponential splines to high-performance interpolating algorithms," *Journal of Computational and Applied Mathematics*, vol. 224, no. 1, pp. 383–396, 2009.

[18] M.-J. Lai and L. L. Schumaker, "On the approximation power of bivariate splines," *Advances in Computational Mathematics*, vol. 9, no. 3-4, pp. 251–279, 1998.

[19] D. Schmitter, A. Roche, B. Maréchal, D. Ribes, A. Abdulkadir, M. Bach-Cuadra, A. Daducci, C. Granziera, S. Klöppel, P. Maeder, R. Meuli, and G. Krueger, "An evaluation of volume-based morphometry for prediction of mild cognitive impairment and Alzheimer's disease," *NeuroImage: Clinical*, vol. 7, pp. 7–17, 2015.

[20] D. Schmitter, R. Delgado-Gonzalo, G. Krueger, and M. Unser, "Atlas-free brain segmentation in 3D proton-density-like mri images," *International Symposium on Biomedical Imaging (ISBI)*, pp. 629–632, 2013.